21st Australasian Fluid Mechanics Conference
Adelaide, Australia
10-13 December 2018

Transient Start-up of a Sonic Jet in Hypersonic Crossflow

W. A. Miller[1], C. J. Doolan[2], P. R. Medwell[1] and M. Kim[3]

[1]School of Mechanical Engineering, University of Adelaide, South Australia 5005, Australia
[2]School of Mechanical and Manufacturing Engineering, University of New South Wales, New South Wales 2052, Australia
[3]Astronautics Research Group, University of Southampton SO17 1BJ, UK

Abstract

This paper presents a numerical study of the transient start-up of a sonic jet into a hypersonic crossflow. Implicit large-eddy simulations were performed using OpenFOAM for a round, sonic, perfect air jet issuing normal to a Mach 5 crossflow, over a flat plate with a laminar boundary layer, at a jet-to-crossflow momentum ratio of 5.3. The evolution of shock and vortex structures, the jet penetration, and the control force have been quantified during the jet start-up. Initially, a lead shock forms, which is quickly deformed and convected downstream by the crossflow. The obstruction caused by the jet leads to formation of barrel shocks, a bow shock, and a Mach disk. The obstruction also results in upstream flow separation, which facilitates the formation of the horseshoe vortices within an upstream re-circulation region. Shear-layer vortices begin to form and shed periodically once the barrel shock structure is established, while longitudinal counter-rotating vortices and wake vortices are not formed until the jet flow has penetrated far downstream. The control force develops on the same time-scale as the longitudinal counter-rotating vortices. An overshoot is observed in the control force after the lead shock and initial jet flow has convected downstream beyond the edge of the plate, and is related to the re-compression of the free-stream flow downstream of the jet outlet, and the development of re-circulation regions.

Introduction

The starting process of a sonic jet in hypersonic crossflow is relevant to reaction control jet applications. When a reaction control jet is operated at high frequency, the start-up process may comprise a signficant portion of the total jet pulse period. Therefore, a detailed understanding of the unsteady flow structures and control force generated during start-up is important to the design of reaction control jet systems. Naumann et al. investigated the unsteady nature of the jet start-up flow-field via wind tunnel experiments [12]. Force data published for jet start-up in an established crossflow is unreliable due to measurement difficulties in the experiment, where oscillations of the model in the crossflow prevented accurate measurement of the control force. Jet start-up was also studied by Chamberlain et al. [2] and Dash et al. [3], who investigated reaction control of the US Army THAAD missile. The flight conditions of interest were Mach 3 – 8, at altitudes around 15 – 45 km. When the chamber pressure was increased linearly from 30% to 100% into a Mach 3 free-stream with a zero degree angle-of-attack, the shock structure developed very quickly, while the development of the wake structure behind the jet takes place over a longer time-period. The rapid development of the shock structure caused an initial overshoot in the control force. Soon afterwards, the jet shock wrapped around the vehicle, creating a high pressure region underneath the vehicle that counteracts the control force. As the wake structure establishes, the low pressure wake completes the aerodynamic force balance, resulting in a steady control force. Ebrahimi [4] simulated the start-up and shut-down of a supersonic jet in a hypersonic ($M_\infty = 5$) freestream at altitudes of 19 – 35 km. This work predicted a large overshoot in the control force, with a settling time corresponding to $\tau \approx 100$, where τ is a non-dimensional time, $\tau = t \times U_\infty / d_j$, for free-stream velocity, U_∞, and jet diameter, d_j. A large steady interaction force is caused by the finned missile geometry trapping the high pressure jet fluid. The magnitude of the control force overshoot depends on the jet-to-crossflow pressure ratio, but the settling time and shut-down time does not. The use of a RANS turbulence model prevents detailed analysis of flow structures to identify the cause of the overshoot and the settling time, as RANS simulations are unable to sufficiently resolve the unsteady, turbulent flow features. Recent work by Despirito [6] focused on transient forces on a generic missile in supersonic flow during jet start-up and shut-down. For a jet pulse with a 10% rise and fall time, the transonic and supersonic flow conditions show significant differences. In a supersonic crossflow at sea-level, the maximum jet force is reached after $\tau \approx 160$, while in transonic crossflow at sea-level, it takes $\tau \approx 220$ with a much larger overshoot. Each of the studies investigating jet start-up have used a cylindrical missile geometry. This complicated geometry, combined with the use of RANS turbulence models, means that detailed understanding of the jet start-up and shut-down processes has not been achieved. The present work aims to provide a detailed understanding of the flow structures generated during the start-up of a sonic jet in hypersonic crossflow over a flat plate, with a laminar in-flow boundary layer.

Numerical Setup

The governing equations for the flow conditions considered in this study are the compressible, unsteady conservation of mass, momentum, and energy. The governing equations were solved in dimensional form using the rhoCentralFoam finite volume solver, which forms part of the OpenFOAM code. A constant Prandtl number of 0.7 was assumed, and viscosity was modeled using Sutherland's law [13]. Only perfect gases were considered. For compressible flows, fluid properties are not only transported by the flow, but also by the propagation of waves. Thus, the numerical scheme used to solve the governing equations requires the flux interpolation to be stabilised based on transport that can occur in any direction. To achieve this, the central-upwind flux reconstruction method of Kurganov et al. [10] was used, with the van Leer limiter [14]. The second-order, implicit Crank-Nicolson method was employed for temporal discretisation [9]. An implicit Large-Eddy Simulation (LES) methodology has been adopted to model turbulence. Numerical schemes that utilise flux-limiting schemes implicitly provide a sub-grid model, of the eddy viscosity type [8]. This approach is referred to as Monotone Integrated Large-Eddy Simulation (MILES), and has shown performance comparable to conventional LES for similar flows, including jets in supersonic crossflow, with a reduced computational cost [1]. The numerical scheme is described in detail in previous work by the authors [11]. The geometric configuration is a sonic jet injected through a circular orifice in a flat plate into a Mach 5 crossflow, with a laminar in-flow boundary layer. The fully established jet flow-field has been investigated previously at the same conditions [5, 11]. A schematic of the geometry is shown in Figure 1, and the free-stream conditions are shown in Table 1. Free-stream conditions were constant, and the simulation was run at a CFL number of

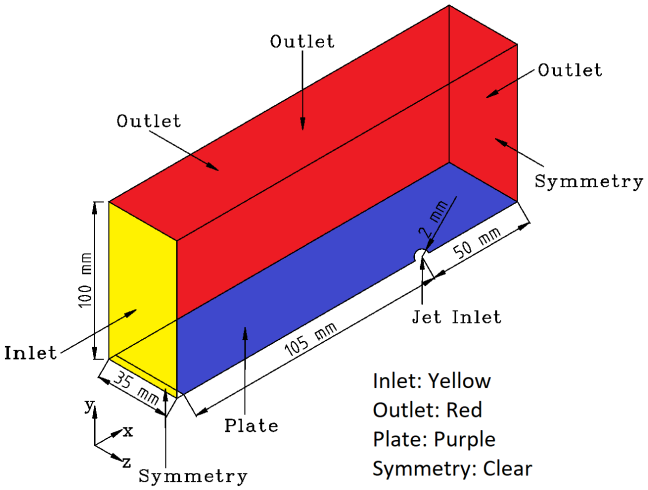

Figure 1: Schematic of the geometric configuration.

Table 1: Free-stream and jet outlet conditions.

M_∞	T_∞ (K)	p_∞ (Pa)	$Re(\times 10^6$ /m)	
5	62	1210	13.1	
M_j	T_j (K)	p_{0j}/p_∞	$Re_{dj}(\times 10^3)$	J
1	250	251	88.5	5.3

0.2. Once a steady, laminar in-flow boundary layer was established, the jet was switched on by instantaneously modifying the jet out-flow static temperature, pressure and velocity, to the values shown in Table 1. The upstream and downstream edges of the domain were a supersonic inlet and Neumann outlet respectively. The plate was modelled as an adiabatic wall, with a circular sonic inlet with jet diameter $d_j = 2$ mm. Geometric symmetry allows the domain to be split in half, with a symmetry condition applied in a plane parallel to the free-stream flow, through the centre-line of the jet. This was shown previously to have minimal influence on the flow structures [11]. Far-field (Neumann) boundary conditions were applied at the top and side to complete the domain, at sufficient distance to capture the relevant flow structures. The jet was assumed to have a "top-hat" velocity profile, and no boundary layer or inlet plenum was modelled. This is a common simplification when considering choked nozzle flows, and has been shown to have little or no effect on the shock formations in the crossflow [1]. The mesh was structured, with hexahedral cells concentrated in the region of the jet orifice, as well as through the boundary layer and on the leading edge of the flat plate. The mesh spacing was increased linearly in all directions from these concentrated regions, and consists of 6.4 M cells. A detailed mesh resolution study and validation against experimental measurements for the steady jet in crossflow was also conducted previously [11].

Flow Structures

The shock and vortex structures in the jet centre-line ($z = 0$) during jet start-up are provided in Figure 2. The initial shock structures consist of a lead shock which travels out into the crossflow, followed by the jet interface, a normal shock (or Mach shock) and a starting vortex, which forms at the edge of the orifice and travels with the jet fluid into the crossflow. The lead shock and Mach shock are deformed and rotated as they extend into the crossflow. The Mach shock is turned downstream to form a Mach disk, while the two oblique barrel shocks also form and are deflected by the crossflow, resulting in different structures between the windward and leeward barrel shocks. The starting vortex continues to develop at either end of the Mach disk, and the plane of this vortex is also rotated by the crossflow, to remain parallel with the Mach disk. A recompression shock forms between the leeward barrel shock and the flat plate. This recompression shock breaks away from the leeward barrel shock and moves downstream as the obstruction caused by the jet increases, resulting in recompression of free-stream flow that has travelled around the barrel shocks occuring further downstream. The adverse pressure gradient caused by the jet flow causes the in-flow boundary layer to separate, and a re-circulation region forms upstream of the jet outlet. A pair of counter-rotating horseshoe vortices form in this developing re-circulation region. The region of separated flow upstream of the jet grows more slowly than the downstream region, and this smaller re-circulation region results in a simplified horseshoe vortex structure compared with the fully developed jet. By $\tau = 5$ a reflected shock and a slip line have formed directly downstream of the Mach disk, and extend between the Mach disk and the flow interface. By $\tau = 7$ the barrel shocks and Mach disk resemble those of the fully developed flow-field, the Mach disk height has reached 85% of the fully developed jet, while the upstream region of separated flow remains small, only 19% of the fully developed jet. Upstream of the jet outlet and outside the boundary layer, the bow shock forms at the interface between the jet and crossflow. The lead shock continues to travel radially outward, while the recompression shock separates from the leeward barrel shock, but remains beneath the Mach disk, and the slip line developed downstream of the Mach disk continues to extend downstream with the flow interface. The upstream starting vortex has rotated and now travels approximately parallel with the crossflow, while trailing vorticity continues to form at the upstream barrel shock, in the shear-layer between the upstream starting vortex and the jet outlet. From $\tau = 7$, the starting vortex begins to separate from the Mach disk, as it convects downstream. At the same time, the trailing vorticity rolls-up, leading to the formation of a second vortex, which can be identified as a jet shear-layer vortex at $\tau = 10$. This second vortex begins to form above the stagnation point, which remains close to the jet outlet, due to the small separated flow region upstream of the jet outlet. This forming shear-layer vortex deforms the bow shock and windward barrel shock.

At $\tau > 10$, the starting vortex continues to detach from the windward barrel shock and Mach disk, and convects downstream. This starting vortex is accompanied by a counter-rotating vortex, which originates in the re-circulation region on the flat plate, at the upstream edge of the jet orifice. During the early stages of flow development, the upstream separated flow region is not fully developed. As a result, the jet shear-layer vortices form much closer to the jet outlet. The proximity of the shear-layer to the re-circulation vortex causes the development of distinct counter-rotating vortices which shed with the conventional shear-layer vortices as a counter-rotating pair. This counter-rotating shear-layer vortex behavour was observed by Won et al. [15] for a sonic jet in supersonic crossflow with a turbulent in-flow boundary layer, but has not been observed in other studies. The phenomenon appears to be related to the upstream separated flow region, which affects the proximity of the shear-layer vortex formation to the jet outlet. If the upstream separated region is sufficiently small, the jet shear-layer vortices will form close to the jet outlet, in close proximity to the re-circulation vortex, which has rotation opposite the jet shear-layer vortices. The result is the formation of counter-rotating pairs of shear-layer vortices, rather than a single distinct shear-layer vortex as conventionally described. This fits well with the observation of Won et al. [15], that the negative span-wise vorticity scales with free-stream velocity, while positive span-wise voriticity scales with jet exit velocity. At $\tau = 20$, the lead shock has reached the domain outlet ($x/d_j = 25$), while the slip line has extended further downstream from the Mach disk, to the flow interface,

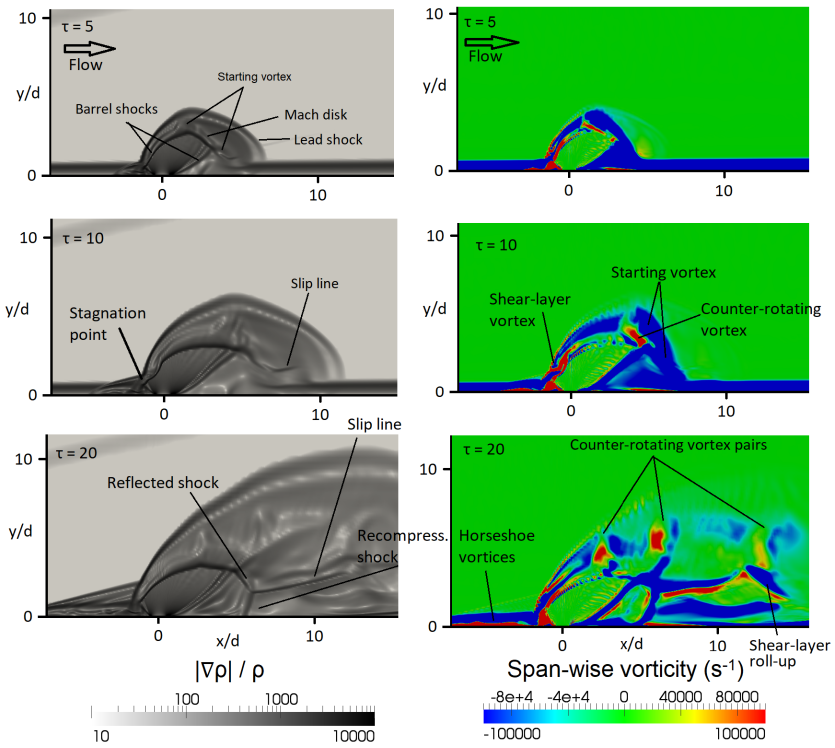

Figure 2: Contours of instantaneous density gradient magnitude and instantaneous span-wise vorticity in the plane of symmetry during jet start-up.

at $x/d_j \approx 15$. At this time, the recompression shock, reflected shock, and slip line all converge to a single point. The barrel shocks and Mach disk are fully developed, the Mach disk height has reached that of the fully established jet. The upstream separation region continues to grow, and the bow shock continues to form as the lead shock expands radially from the jet orifice. For $\tau > 20$, the slip line is deformed by shear-layer vortex shedding, and the unsteady recompression shock can no longer be clearly identified in the plane of symmetry. The upstream starting vortex weakens as it travels downstream, while the downstream flow-field continues to develop, with the flow interface reaching the domain outlet at $\tau \approx 40$. At this time, the upstream separated flow region has extended further but continues to develop, the bow shock has fully developed, and the thicker separated boundary layer causes the stagnation point to be located further from the jet outlet, and further from the flat plate. The development of the upstream separated region continues until $\tau \approx 60$, and counter-rotating shear-layer vortices are observed. For $\tau > 60$, the upstream re-circulation region is fully formed, the shear is reduced at the stagnation point, and jet shear-layer vortices are not observed close to the jet orifice. This prevents the formation of counter-rotating shear-layer vortices, as the vorticity formed in the re-circulating vortex remains confined to this region. This marks the transition to a quasi-steady, fully established jet.

Penetration

Jet penetration was measured as the maximum height in the y direction of the instantaneous stream-line that originates from the centre of the jet outlet. A plot of penetration vs. time is provided in Figure 3. Time-averaged penetration data for the fully established jet from [11] is also included for comparison. During the initial start-up, while $\tau < 10$, the penetration increases with time, at a decreasing rate. This corresponds to the period where the barrel shocks and Mach disk are extending out from the jet orifice and being turned by the crossflow. At $\tau = 10$, the jet barrel shocks and Mach disk are formed, and jet penetration reaches the time-averaged value of $y/d_j = 5.6$. When this occurs, the rate of change of penetration depth decreases rapidly. A small overshoot in jet penetration is observed during the period $10 < \tau < 50$, while maximum jet penetration is not achieved until $\tau = 40$, with a value of $y/d_j = 6.6$, corresponding to an 18% overshoot of the time-averaged value. Maximum penetration is not observed immediately, penetration reaches a steady value of $y/d_j = 6.2$ (10% overshoot) during the period $20 < \tau < 30$, before increasing again to the maximum value at $\tau = 40$. Peak penetration corresponds to the intial jet flow, which continues to expand downstream of the jet orifice, as the lead shock moves toward the domain outlet. Penetration peaks at $\tau = 40$, when the initial jet flow reaches the domain outlet. The extended period of overshoot from $10 < \tau < 50$ is maintained during the time period where the lead shock is moving toward the domain outlet, and the upstream separated flow region and the bow shock are still forming. This behaviour differs from pulsed jets in subsonic crossflow, where increased penetration is linked to formation of strong shear-layer vortex rings which penetrate deeply into the crossflow [7]. Here, maximum penetration is observed during the start-up period, as the bow shock is still forming. At times $\tau > 40$, the jet penetration returns to the time-averaged value, with small oscillations about the mean corresponding to the instantaneous flow structure. Instantaneous penetration slightly increases at shear-layer vortex shedding events, for example, at $\tau = 80$.

Interaction Force

The resulting interaction force, F, can be obtained by integrating the surface pressure. This results are provided in Figure 4, in non-dimensional form, i.e. $C_F = F/\rho_j A_j U_j^2$, where ρ_j, A_j, and U_j and the jet density, area, and velocity respectively. Jet thrust coefficient and jet interaction force coefficient for the fully established jet are provided for comparison. Initially, the jet interaction force increases linearly over the period $0 < \tau < 40$. At $\tau = 40$, the interaction force overshoots the steady jet value by 18%, with a peak value of $C_F = 1.064$. The magnitude and

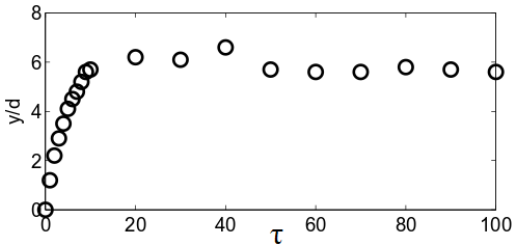

Figure 3: Jet penetration vs. time during jet startup. ○: Instantaneous penetration, Dash line: time-averaged penetration.

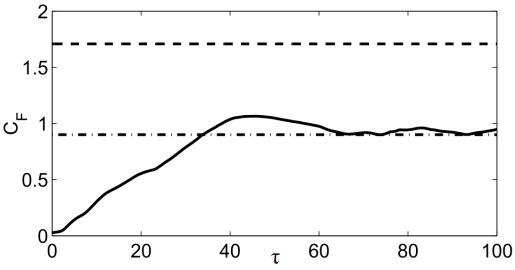

Figure 4: Jet thrust coefficient (Dash line), interaction force coefficient (Solid line), and time-averaged interaction force coefficient (Dot-dash line).

timing of this overshoot directly corresponds to the peak penetration observed during the jet start-up, indicating that penetration and control force are strongly linked. However, the nature of the time dependent force differs from the jet penetration. The interaction force of the fully established jet is not reached until $\tau = 35$, while jet penetration exceeds that of the fully established jet within $\tau < 10$. The penetration is driven by the establishment of the barrel and Mach shocks, while the interaction force is driven by the formation of the bow shock, and the expansion of the downstream low pressure region behind the lead shock. The bow shock and downstream low pressure region are established over $\tau \approx 50$; after this time, the downstream region resembles the fully developed flow. As a result, the interaction force evolves over the same time period. During the period $50 < \tau < 60$, the interaction force continues to decrease, corresponding to the continued formation of the upstream recirculation region, which is a region of high pressure. Small variations are also observed in the interaction force at later times, corresponding to the formation and motion of individual vortex structures. While the linear increase in control force is observed over a longer period than the increase in penetration, the development of the jet interaction force occurs over a shorter time period than observed in previous work [4, 6]. Here, the faster development time is due to the simplified geometry of a flat plate, compared with a finned missile configuration used previously. With a finned missile, the shocks wrap around the cylindrical body, and a significant force overshoot is observed while the lead shock passes over the fins. Force development is also dependent on the size of the missile or flat plate – a larger downstream area relative to the jet diameter will result slower development of the interaction force. However, this study allows the link to be drawn between the interaction force, and the development of specific flow structures (bow shock, lead shock etc.) not previously documented.

Conclusions

The start-up of a reaction control jet can significantly affect the overall control force when the jet is pulsed at hgh frequency. During the start-up period, shear-layer vortices are developed in counter-rotating pairs, due to the proximity of the stagnation point to the jet orifice. If the upstream separated region is sufficiently small, the jet shear-layer vortices will form close to the jet outlet, in close proximity to the re-circulation vortex, which has rotation opposite the jet shear-layer vortices. The result is the formation of counter-rotating pairs of shear-layer vortices, rather than a single distinct shear-layer vortex as conventionally described. Jet penetration shows an 18% overshoot at $\tau = 40$, with increased penetration caused by the expansion of initial jet flow behind the lead shock. The interaction force is also driven by the lead shock. Overall, the interaction force developed during start-up can be characterised as a lightly damped second order system, with an 18% overshoot, and a settling time of $\tau \approx 60$.

References

[1] Andre, T., A. Durant, and I. Fedioun (2017). Numerical study of supersonic boundary layer transition due to sonic wall injection. AIAA Journal 55 (5), 1530 1547.

[2] Chamberlain, R., D. McClure, and A. Dang (2000). CFD Analysis of Lateral Jet Interaction Phenomena for the THAAD Interceptor. In *AIAA Aerospace Sciences Meeting and Exhibit*, Reno, NV (AIAA-2000-0963).

[3] Dash, S. M., E. R. Perrell, S. Arunajatesan, and C. Kannepalli (2000). Lateral Jet Aerodynamic Interaction Simulations for Dynamic Pressure Loads. In *AIAA Aeroacoustics Conference*, Lahaina, HI (AIAA-2000-2036).

[4] Ebrahimi, H. B. (2000). Numerical Simulation of Transient Jet-Interaction Phenomenology in a Supersonic Freestream. AIAA Journal of Spacecraft and Rockets 37, 713 719.

[5] Erdem, E. (2011). Active Flow Control Studies at Mach 5: Measurement and Computation. Ph. D. thesis, University of Manchester, School of Mechanical, Aerospace and Civil Engineering.

[6] DeSpirito, J. (2012). Transient Lateral Jet Interaction Effects on a Generic Fin-Stabilized Projectile. In *AIAA Applied Aerodynamics Conference*, New Orleans, LA (AIAA-2012-2907).

[7] Gevorkyan, L., T. Shoji, D. R. Getsinger, O. I. Smith, and A. R. Karagozian (2016). Transverse jet mixing characteristics. Journal of Fluid Mechanics 790, 237 274.

[8] Grinstein, F. F. and C. Fureby (2007). On flux-limiting-based implicit large eddy simulation. Journal of Fluids Engineering 129, 1483 1492.

[9] Jasak, H. (1996). Error Analysis and Estimation for the Finite Volume Method with Applications to Fluid Flows. Ph. D. thesis, Imperial College of Science, Technology and Medicine, Department of Mechanical Engineering.

[10] Kurganov, A., S. Noelle, and G. Petrova (2001). Semidiscrete Central-Upwind Schemes for Hyperbolic Conservation Laws and Hamilton-Jacobi Equations. SIAM Journal of Scientific Computing 23 (3), 707 740.

[11] Miller, W. A., P. R. Medwell, C. J. Doolan, and M. Kim (2018). Transient interaction between a reaction control jet and a hypersonic crossflow. Physics of Fluids 30, 046102.

[12] Naumann, K. W., H. Ende, G. Mathieu, and A. George (1993). Millisecond Aerodynamic Force Measurement with Side-Jet Model in the ISL Shock Tunnel. AIAA Journal 31, 1068 1074.

[13] Sutherland, W. (1893), The viscosity of gases and molecular force, Philosophical Magazine, S. 5, 36, pp. 507 531.

[14] van Leer, B. (1974). Towards the Ultimate Conservative Difference Scheme II. Monotonicity and Conservation Combined in a Second Order Scheme. Journal of Computational Physics 14, 361 370.

[15] Won, S., I. Jeung, B. Parent, and J. Choi (2010). Numerical investigation of transverse hydrogen jet into supersonic crossflow using detached-eddy simulation. AIAA Journal 48 (6), 1047 1058.